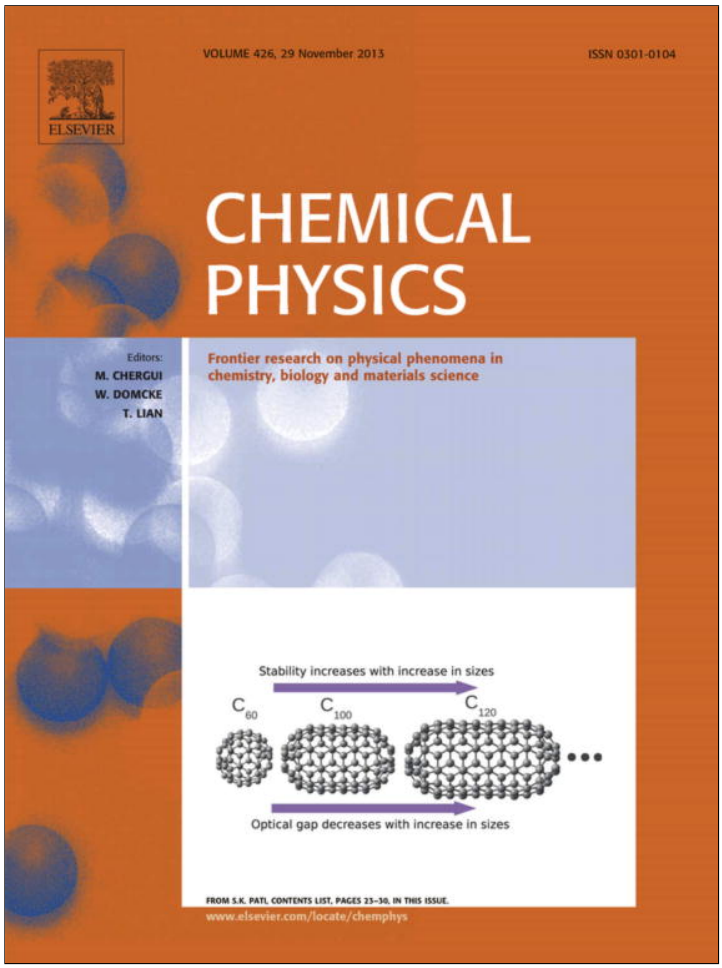

Chemical Physics 426 (2013) 48–53

Contents lists available at ScienceDirect

Chemical Physics

journal homepage: www.elsevier.com/locate/chemphys

Endohedral complexes of Polyhedral Oligomeric Silsesquioxane (POSS) cages with transition metal dihydrides

Xiqiao Wang, John Corn, Frank Hagelberg *

Department of Physics and Astronomy, East Tennessee State University, Johnson City, TN 37614, USA

ARTICLE INFO

Article history:
Received 12 July 2013
In final form 12 September 2013
Available online 12 October 2013

Keywords:
Atomic and molecular clusters
Nanostructures
Hydrogen storing systems
Metal hydrides

ABSTRACT

Polyhedral Oligomeric Silsesquioxane (POSS) cages are investigated in terms of their potential to enclose small metal hydrides, with the objective of defining conditions that maximize the number of encapsulated hydrogen atoms. Systems of the form $MH_{2n}@T_m$, where $n = 1–3$, $m = 8, 10$, and M comprises metal atom species of the groups IV, VI, VIII, X, and XII, are studied by methods of *ab initio* and density functional theory (DFT). The resulting composites are categorized with respect to their structural and energetic features. For $MH_2@T_8$, it is found in all cases considered that including MH_2 into the POSS cage is an endothermic process. For $MH_2@T_{10}$ and M = Ti, Ru, Os, Pt, inclusion of the MH_2 guest into the cage turns out to be exothermic, and also leaves the cage intact. For $MH_4@T_m$, this behavior is only observed for one system, $OsH_4@T_{10}$.

1. Introduction

Nanostructures are of great interest as hydrogen storage media [1]. Thus, proposals to enclose hydrogen in carbon nanostructures, such as fullerenes [2] or carbon nanotubes, have been made. Greater storage densities of endohedral hydrogen may be achieved if pure hydrogen species are replaced by metal hydrides [2,3]. As demonstrated by recent density functional theory (DFT) studies [2], hydrogen-rich metal polyhydrides, such as ScH_{15} or ZrH_{16}, which are unstable in the gas phase, can be stabilized by inclusion into C_{60}. Several authors [4–9] have dealt with core species of the form XH_4, where X stands for a group IV (A or B) atom, in C_{60} or larger fullerenes. Thus, semi-empirical calculations were carried out for X = C, Si [4], molecular mechanics [5] and DFT with subsequent second-order Moller–Plesset perturbation theory (MP2) treatment at equilibrium geometry was applied to study the case of X = C [6–8], and DFT was also used to investigate X = Ge [9], and X = Zr [2]. As demonstrated by comparison with the respective gas phase species, the XH_4 structures containing C and Si remained almost unchanged upon encapsulation while sizable compression was reported for X = Ge and Zr. The formation of $XH_4@C_{60}$ (where the @ symbol stands for *encapsulated in*) was found to be weakly exothermic at the MP2 level for X = C, and distinctly exothermic for X = Ge.

In this contribution, we discuss Polyhedral Oligomeric Silsesquioxane (POSS) cages as potential enclosures for metal hydride encapsulation. A POSS monomer is a cage molecule of composition $(RSiO_{3/2})_{2n}$, with $n = 4,5,6,\ldots$, and R as a hydrogen atom or an organic or inorganic ligand. The notation T_n – POSS abbreviates the structural formula $n(HSiO_{3/2})$. Thus, T_8 (Octahydridosilsesquioxane) consists of eight Si atoms located at the corners of a cube, twelve O atoms bridging between them, and a hydrogen atom attached to each Si atom. Inorganic–organic hybrid systems, generated by adding POSS cages or their derivatives to organic polymers have found numerous applications in materials science and catalysis [10–20]. The resulting nanocomposites are harder than the original polymers [21], they often have higher mechanical strength and exhibit enhanced decomposition and glass transition temperatures [22–25].

While, to our knowledge, metal hydride encapsulation into POSS cages has not been the subject of a systematic computational study so far, various results exist on POSS cages with endohedral hydrogen, both atomic [26,27] and molecular [26], and also with endohedral metal atoms [28–30]. Maiti et al. [26] report DFT computations on the insertion process of a physisorbed H radical into $(CH_3SiO_{3/2})_8$, using a double-numeric polarized basis set in conjunction with a gradient-corrected exchange correlation functional. This approach leads to an energy barrier of 1.2 eV for the transition into the cage which proceeds through the Si_4O_4 ring nearest to the H radical. This insertion process turned out to be slightly endothermic, with an energy difference of about 0.2 eV between endohedral and exohedral configurations.

Several transition metal species, both in atomic and ionic form, have been investigated as guest units of the T_8 cage by use of DFT [29]. From comparison between the endohedral complex and the empty T_8 host in separation from the guest, the transition metal atom or ion insertion was determined to be endothermic for most

* Corresponding author. Tel.: +1 423 439 6725.
E-mail address: hagelber@etsu.edu (F. Hagelberg).

0301-0104/$ - see front matter © 2013 Elsevier B.V. All rights reserved.
http://dx.doi.org/10.1016/j.chemphys.2013.09.003

species, with some group 4 transition metal ions (Fe^+, Co^+, Ni^+, Cu^+) as exceptions. Insertion of alkali metal guests has been explored by DFT computation for T_8 [31] and T_{10} [28] cages and found to be endothermic for all atomic species, while some host–guest combinations turned out to be exothermic for the corresponding cations.

In this work, we consider complexes of the form $MH_{2n}@T_m$, where M stands for various metal atoms from groups IV, VI, VIII, X, and XII, and $m = 8$, 10. While we focus mostly on dihydrides ($n = 1$), the cases $n = 2$, 3 will be included for some selected metal atom species. Each composite will be discussed in terms of two guiding questions: 1. To what extent does the guest species modify the cage?, and 2. Is the insertion of this species an endothermic or exothermic process? Further, the free and the encapsulated MH_{2n} molecule will be compared.

2. Computational method

For all systems considered in this work, geometry optimizations were performed by use of the hybrid B3LYP functional [32,33] in conjunction with the frozen core CEP basis set [34]. Stable isomers were identified by frequency analysis. For energy comparison, perturbation theory at second order in the electron correlation effect (MP2) was carried out at equilibrium geometries.

For the metal dihydride molecules, additional computations were performed with the much more extensive 6-311G**(pdf) basis set, wherever available. For some systems (TiH_2, CrH_2), the calculations employing the two different basis sets led to substantially different bond angle assignments. In those cases the result obtained when using the larger basis set was adopted.

The ability of the CEP basis set to represent the endohedral systems considered here was assessed by comparing the optimized geometries for the clusters $MH_2@T_N$ with M = Fe, Ni and N = 8, 10 as resulting from B3LYP/CEP and B3LYP/6-31G treatment. The bond length in the structures obtained from these two approaches turned out to differ from each other by less than one per cent.

For all $MH_{2n}@T_m$ ($m = 8,10$) systems, inclusion energies E_{inc} were evaluated according to

$$E_{Inc.} \equiv E_{endo} - (E_{cage} + E_{MH_2}) + \Delta E_{ZP}$$
$$\Delta E_{ZP} \equiv \Delta E_{ZP\_endo} - (\Delta E_{ZP\_cage} + \Delta E_{ZP\_MH_2})$$

Here, E_{endo}, E_{cage}, and E_{MH_2} stand for the total energies of the endohedral structure, the pure T_m ($m = 8,10$), and the metal dihydride guest, respectively, while ΔE_{ZP} denotes the zero-point energy correction.

All systems were investigated in singlet, triplet, and quintet spin configurations. For all endohedral structures included here, the basis set superposition error was eliminated by carrying out counterpoise computations.

3. Results and discussion

In the following, we will first present our results on the metal dihydrides considered in this work and then turn to $MH_{2n}@T_m$ ($n = 1$–3, $m = 8,10$) composites. Specifically, we will comment on metal dihydrides in a T_8 cage, and on metal dihydrides as well as polyhydrides enclosed in T_{10}.

3.1. Pure metal dihydrides

Since the emphasis of this study is on MH_2 as endohedral species, we discuss the pure MH_2 species primarily in terms of its size as compared to the dimensions of T_8 and T_{10} POSS cages.

Table 1 lists the results found by geometry optimization of MH_2 at the B3LYP/CEP-121g or B3LYP/6-311G** level. The ground state multiplicities obtained from these calculations are indicated, along with the equilibrium bond length and bond angles and the total energy at the equilibrium geometry, as evaluated by use of the MP2/CEP-121g method.

Table 1
The ground state of transition metal dihydrides in the gas phase, optimized at the B3LYP/CEP-121g level.

	Multiplicity	Bond length[a]	Bond angle	Ground state energy (MP2/CEP-121g)[a]
TiH_2	3	1.799	124.25	−58.798
ZrH_2	1	1.869	124.81	−47.654
HfH_2	1	1.854	134.28	−49.518
CrH_2	5	1.722	180.00	−87.207
MoH_2	5	1.727	107.72	−68.624
WH_2	5	1.841	170.73	−68.256
FeH_2	5	1.632	155.06	−123.905
RuH_2	3	1.615	59.48	−94.468
OsH_2	5	1.702	141.63	−91.673
NiH_2	3	1.567	180.00	−169.938
PdH_2	3	1.640	134.72	−127.775
PtH_2	3	1.634	133.14	−120.113
ZnH_2	1	1.543	180.00	−226.540
CdH_2	1	1.701	180.00	−167.349
HgH_2	1	1.682	180.00	−154.120

[a] The bond lengths are in Å, the energies in Hartree.

Going from group IV to group XII, we observe a tendency towards linear geometry. All metal dihydrides of group IV are found to have bond angles distinctly smaller than 180° in their most stable equilibrium structures, while all bond angles for the group XII systems considered here are 180°. This trend is correlated with the variation of the metal atom valence electron configuration as one goes from group IV to group XII which changes from a twofold occupied to a completely occupied valence d orbital.

We point out that the present approach (MP2/CEP-121g) yields a spin triplet as the NiH_2 ground state which is separated from the spin singlet by an energy difference of 1.67 eV. Density functional theory methods, in contrast, favor the NiH_2 spin singlet [35,36].

3.2. $MH_2@T_8$ complexes

The pure T_8 cage exhibits T_h symmetry in the gas phase [31,37] and O_h symmetry in solution [38]. In order to evaluate the preferred orientation of the MH_2 moiety in the T_8 cage, various initial geometries were tested. In all cases, the MH_2 molecule was placed into the cage with an initial bond angle of 180°, and with an M—H bond distance as obtained for the pure MH_2 unit. The examined initial structures involved the two H atoms of MH_2 directed towards two diagonally opposite Si atoms (O atoms) of the cage, as well as towards the centers of two opposing faces. Plausibly, the latter configuration emerged as the most stable structural type for $MH_2@T_8$ in all cases. The alternative initial geometries were seen to result either in cage breaking or in the most stable structure, involving the two H atoms located at opposing T_8 faces, as exemplified in Fig. 1 for the case of $RuH_2@T_8$.

Less regular behavior is recorded for complexes containing metal dihydrides that adopt bent structures as spin singlets in the gas phase spin (M = Ti, Zr, Hf, Mo, W). In these cases, the initial structure is found to deviate from the cage center. This displacement leads to stable structures that involve bonding between the metal atom and cage atoms, inducing cage deformation. Fig. 2 illustrates this tendency by the example of $TiH_2@T_8$ where the equilibrium geometry involves a TiH_2 subunit with a bond angle strongly reduced from the gas phase value of 123° to 91° for the endohedral species. The Ti atom approaches the bottom face of the cage, interacting with two O atoms. Moving within group IV from Ti to Hf, we observe a gradual opening of the bond angle from 91° to 167°.

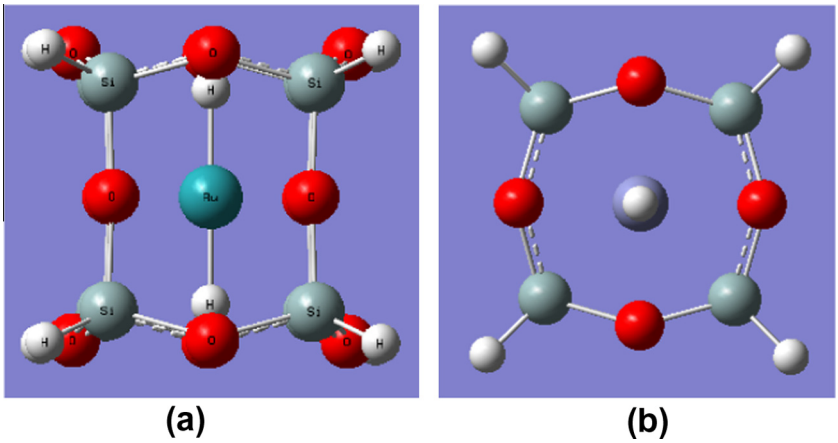

Fig. 1. Most stable structure identified for $RuH_2@T_8$, (a) side view, (b) top view.

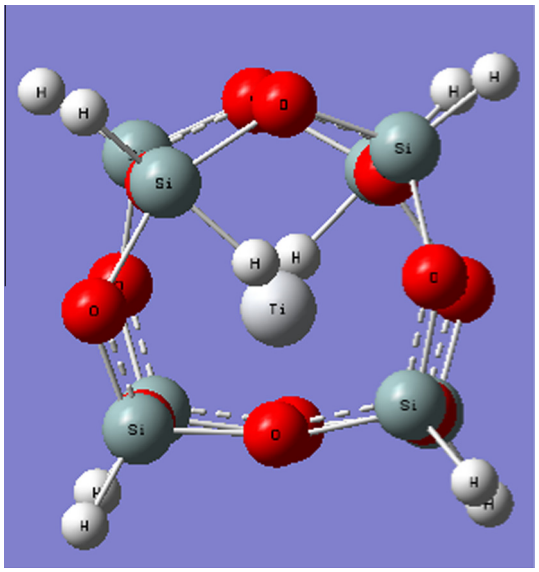

Fig. 2. Equilibrium structure of $TiH_2@T_8$.

In the remaining cases, the MH_2 moiety adopts linear or near-linear form. The endohedral molecule thus defines a cage axis. In most cases considered here, $MH_2@T_8$ stabilizes in orthorhombic symmetry. The complexes containing group X metal atoms (Ni, Pd, Pt), however, are an exception to this rule, as they prefer monoclinic shapes, as illustrated by Fig. 3 for the case of $NiH_2@T_8$.

Comparing the M—H bond lengths of the linear endohedral MH_2 substructures in spin singlet configuration with those of the most stable MH_2 gas phase species we find that the former tend to be shorter than the latter, with bond length reductions ranging from 3.7% (M = W) to 9.0% (M = Cr). The species $OsH_2@T_8$ defines an exception, as the Os—H bond length turns out to be elongated by 1.6% as compared with gas phase structure of lowest energy. There, a bond angle of 110.1° was obtained. A less stable isomer at 180° exhibits a regular bond length reduction of 6.4%.

While deforming the cage, all investigated $MH_2@T_8$ complexes leave the cage intact. From Table 2, however, all of them are endothermic.

3.3. $MH_2@T_{10}$ complexes

The T_{10} gas phase equilibrium structure of minimal energy exhibits D_{5h} symmetry [27]. The defining elements of its architecture are a double five-membered ring (D5R) frame with two $(—SiH—O—)_5$ rings, and five $(—SiH—O—)_4$ rings. For the present investigation, the crucial distinction between the T_{10} and the T_8 cage lies in the greater volume of the former. Consequently, the MH_2 guest is more likely to adopt a geometry close to its gas phase structure in the T_{10} than in the T_8 cage. In terms of the initial geometry for $MH_2@T_{10}$ optimization, we define two prototypes. In the first (*vertical*) alternative, the fivefold axis of the pure cage lies in

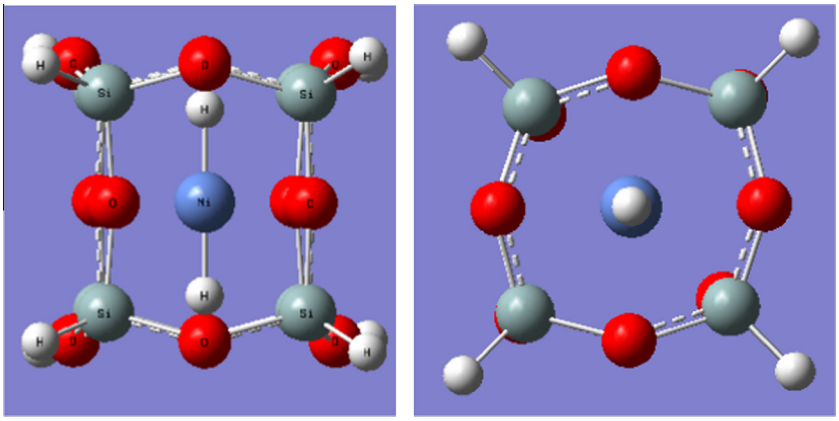

Fig. 3. Equilibrium structure of $NiH_2@T_8$.

Table 2
The Zero Point corrected inclusion energy (Hartree) and HOMO–LUMO gap of ground state $MH_{2n}@T_m$ (eV) calculated at the MP2/CEP-121g level of theory.

	Multiplicity	Inclusion energy	HOMO–LUMO gap
(a) m = 8, n = 1			
$TiH_2@T_8$	1	0.097	0.396
$ZrH_2@T_8$	1	0.127	0.306
$HfH_2@T_8$	3	0.156	0.493
$CrH_2@T_8$	3	0.106	0.454
$MoH_2@T_8$	1	0.143	0.421
$WH_2@T_8$	1	0.108	0.401
$FeH_2@T_8$	3	0.126	0.506
$RuH_2@T_8$	1	0.091	0.452
$OsH_2@T_8$	1	0.115	0.451
$NiH_2@T_8$	1	0.117	0.507
$PdH_2@T_8$	1	0.139	0.408
$PtH_2@T_8$	1	0.135	0.450
$ZnH_2@T_8$	1	0.160	0.533
$CdH_2@T_8$	1	0.252	0.498
$HgH_2@T_8$	1	0.264	0.491
(b) m = 10, n = 1			
$TiH_2@T_{10}$	1	−0.010	0.399
$ZrH_2@T_{10}$			
$HfH_2@T_{10}$			
$CrH_2@T_{10}$	1	0.075	0.481
$MoH_2@T_{10}$	1	0.067	0.409
$WH_2@T_{10}$			
$FeH_2@T_{10}$	1	0.046	0.509
$RuH_2@T_{10}$	1	−0.030	0.474
$OsH_2@T_{10}$	1	−0.012	0.428
$NiH_2@T_{10}$	1	0.007	0.467
$PdH_2@T_{10}$	1	−0.007	0.379
$PtH_2@T_{10}$	1	−0.006	0.469
$ZnH_2@T_{10}$	1	0.052	0.523
$CdH_2@T_{10}$	1	0.091	0.498
$HgH_2@T_{10}$	1	0.089	0.494
(c) m = 10, n = 2			
$OsH_4@T_{10}$	1	−0.009	0.478
$RuH_4@T_{10}$	1	0.007	0.506
$PtH_4@T_{10}$	1	0.052	0.452
$TiH_4@T_{10}$	1	0.202	0.430
(d) m = 10, n = 3			
$OsH_6@T_{10}$	1	0.064	0.488

the plane defined by the metal dihydride, in the second (*horizontal*), that plane is oriented perpendicular to the fivefold axis.

For illustration, we describe the two stable $OsH_2@T_{10}$ structures that emerge from these two basic arrangements, as shown in Fig. 4. The horizontal orientation leads to the ground state geometry. In the resulting structure, Os localizes at a position midway between the two fivefold rings, interacting with one O atom within the five-O-atoms layer that separates these two rings (see Fig. 4(b)). The vertical alternative, in contrast, yields an isomer where the Os atom adopts a position close to one of the fivefold rings, yet still within the cage (see Fig. 4(a)). It bonds to an Si atom of this ring, namely the one in maximum distance from the H_2 pair of OsH_2. If the horizontal geometry is realized, in some cases, the metal-cage interactions characteristic for $MH_2@T_{10}$ lead to strong deformations of the cage (M = Ti), or to cage breakage (M = Zr, Hf, W).

Exothermal complexes with intact cages were selected for further investigations, related to their capacity of accommodating larger numbers of hydrogen atoms than two. Specifically, guest species of the form MH_n, with $n = 4, 6$, were included in this research. From Table 2(b), the zero-point energy corrected inclusion energies are negative for five $MH_2@T_{10}$ complexes among those considered here, namely the species with M = Ti, Ru, Pd, Os, and Pt. We excluded $PdH_2@T_{10}$ from further analysis, since in this case, the metal dihydride is not completely enclosed by the cage, in contrast to the four other species.

Modeling $MH_4@T_{10}$ (M = Ti, Ru, Os, Pt) we defined three initial arrangements, corresponding to different initial shapes of the MH_4 subsystem. Specifically, MH_4 was enclosed in a tetrahedral, seesaw, and square structure [39]. All calculations were performed at the B3lyp/cep-121g//mp2/cep-121g level of theory. To confirm the preference of the spin singlet state, the spin multiplicities 1, 3, and 5 were considered for one selected system ($OsH_4@T_{10}$), while the spin singlet configuration was assumed for the remaining species.

The most stable $MH_4@T_{10}$ (M = Ti, Ru, Os) structures are derived from an initial geometry that contains MH_4 as a square. The most stable $PtH_4@T_{10}$ structure is derived from an initial geometry that contains PtH_4 at a seesaw. The final structure of MH_4 as guest species in T_{10} deviates strongly from the initial, with the exception of M = Pt, where the seesaw is preserved. A typical $MH_4@T_{10}$ geometry is displayed in Fig. 5 by the example of M = Os.

Comparing the M—H bond lengths of MH_4 (M = Ti, Ru, Os, Pt) as realized in the cage with those in the free molecule, we note a marked reduction in each one of the four cases. From Table 3, the bond lengths decrease ranges between 2% (M = Ru) and 8% (M = Pt). Thus, the MH_4 moiety exists in a more compact configuration when trapped in the T_{10} cage than in the gas phase. More detailed geometric information on the gas phase ground state of MH_4 (M = Ti, Ru, Os, Pt) is contained in Table S-3.

From Table 2(b), our computations yield only one exothermic system, namely $OsH_4@T_{10}$. Comparing the four contenders $MH_4@T_{10}$ (M = Ti, Ru, Os, Pt), we note that they realize different cage-core interaction models. The Pt containing species

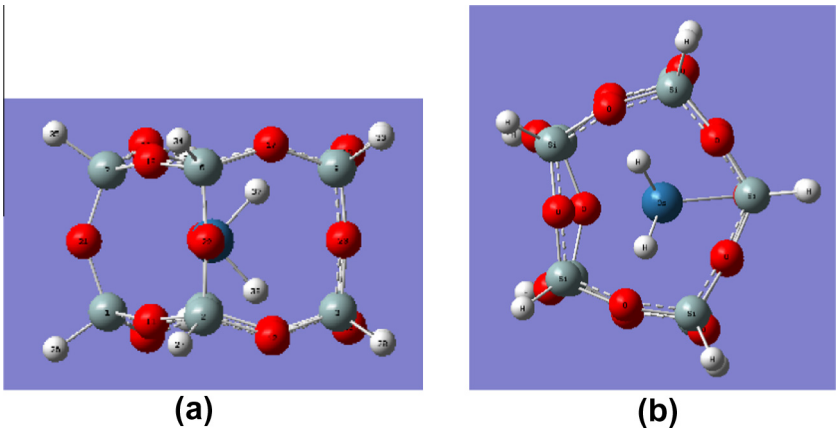

Fig. 4. Equilibrium structures of $OsH_2@T_{10}$, derived from the vertical (a) and the horizontal (b) orientation of OsH_2 in the initial geometry.

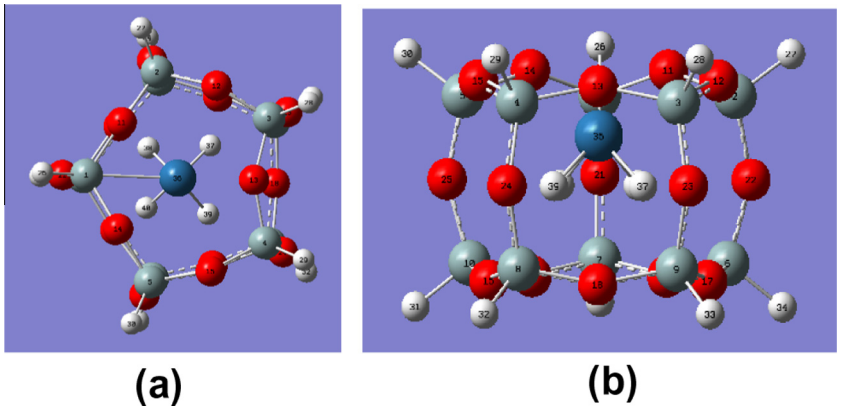

Fig. 5. Equilibrium structure of $OsH_4@T_{10}$. (a) Top view, (b) side view.

Table 3
Geometric parameters pertaining to the MH_4 guest species (M = Ti, Ru, Os, Pt) and the encapsulating T_{10} cages. The expansion ratio of the T_{10} cage is calculated from the difference between the averaged bond lengths in the pure and the encapsulating T_{10} cage.

(a) Bond lengths (Å) of ground state MH_4 in the gas phase

	Bond 21	Bond 31	Bond 41	Bond 51	Averaged bond length
OsH_4	1.603	1.603	1.603	1.604	1.603
RuH_4	1.572	1.571	1.571	1.572	1.571
PtH_4	1.885	1.535	1.888	1.570	1.720
TiH_4	1.703	1.703	1.702	1.702	1.702

(b) Averaged M—H bond lengths and cage expansion ratios of $MH_4@T_{10}$

MH_4	Multiplicity	Averaged bond length	T_{10} cage expansion ratio
OsH_4	1	1.555	0.027
RuH_4	1	1.538	0.019
PtH_4	1	1.569	0.024
TiH_4	1	1.663	0.033

accommodates the metal atom at the cage center, corresponding to strongly delocalized bonding between the metal atom and the cage. A different model prevails for $RuH_4@T_{10}$, as the Ru atom, while still being located close to the central cage axis, tends distinctly towards the lower rather than the upper face, displaying higher bond selectivity than found in the case M = Pt. Lastly, the metal-cage interaction encountered in $OsH_4@T_{10}$ is most selective. The OsH_4 complex attaches to the upper face, where Os forms a bond with one of the respective Si atoms. The Os—Si bond distance is 2.55 Å, the lowest of all M–Si distances observed in the $MH_4@T_{10}$ (M = Ti, Ru, Os, Pt) clusters considered here. As yielded by natural bond orbital analysis, the charge transfer between Os and Si is almost negligible, suggesting predominantly covalent character of the Os—Si bond. Similar observations apply to $TiH_4@T_{10}$ where, however, the T_{10} cage expansion is found to be significantly higher than for M = Os. From our calculations, the $OsH_4@T_{10}$ configuration turns out to be of maximum stability among the models compared here.

The exothermic character of $OsH_4@T_{10}$ provokes the question if the choice M = Os allows for loading the T_{10} cage with an even higher number of H atoms than four. In response, we considered the system $OsH_6@T_{10}$, using the same methodology as for $MH_4@T_{10}$. Once more, singlet, triplet, and quintet spin states were included in this study, with the singlet emerging as most stable. A preceding optimization of the pure OsH_6 molecule yielded a deformed octahedral unit, involving four (two) Os—H bonds with a bond distance of 1.60 (1.68) Å. This geometry becomes substantially distorted when MH_6 is embedded into the T_{10} cage, as shown in Fig. 6.

From Table 2(d), the optimized $OsH_6@T_{10}$ unit is highly endothermic.

Our observations suggest that, among the metal species from groups IV, VI, VIII, X, and XII included in this work, Os is capable of accommodating a maximum number of H atoms as guest species in the T_{10} cage.

As illustrated in Fig. 7 by the example of $OsH_4@T_{10}$, both the HOMO and the LUMO state are strongly dominated by the metal hydride guest unit in all systems explored in this study. This reflects a general feature of the metal-hydride-POSS complexes discussed in this work, as substantiated by the trends in the HOMO–LUMO gaps listed in Table 2. Comparing the gaps for the $MH_2@T_8$ and $MH_2@T_{10}$, we see that the gaps vary strongly with

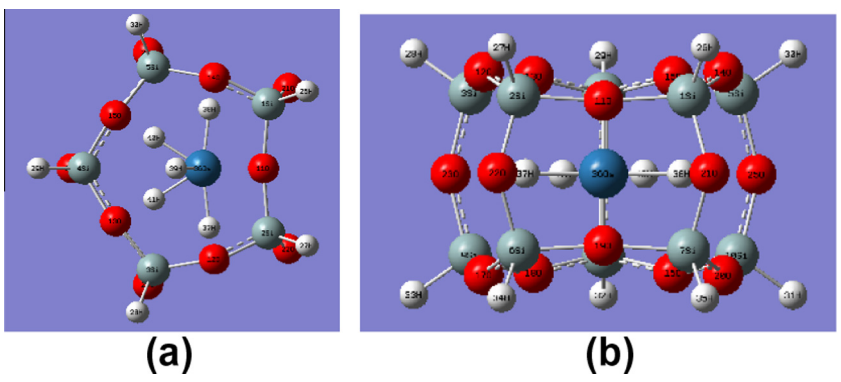

Fig. 6. Equilibrium structure of $OsH_6@T_{10}$. (a) Top view, (b) side view.

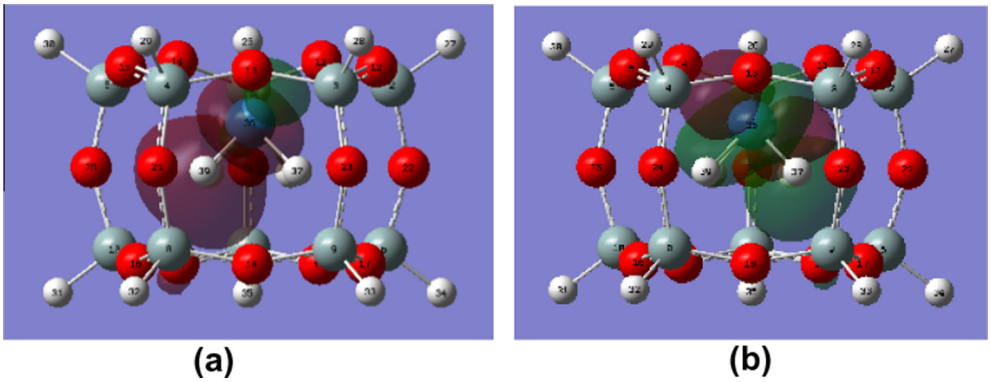

Fig. 7. Representation of the HOMO (a) and the LUMO (b) of $OsH_4@T_{10}$.

the metal species. For a specific M, however, the difference between the gaps is markedly smaller, not exceeding eight per cent.

4. Conclusions and outlook

Comparative investigations on the geometric features and the stabilities of $MH_{2n}@T_m$ systems, where $n = 1–3$, $m = 8$, 10, and M denotes metal atom species of the groups IV, VI, VIII, X, and XII, have been performed by methods of quantum chemistry. In all cases considered, including MH_2 into T_8 was found to leave the cage intact but, at the same time, turned out to be an endothermic process. Some clusters studied in this work, however, appear as viable synthetic targets, exhibiting negative inclusion energies. Specifically, for larger composites of the form $MH_2@T_{10}$ with intact cages, the combined unit of cage and guest turned out to be more stable than the separated subsystems in several cases, namely for M = Ti, Ru, Os, Pt. Using this subset of metal atom species, $MH_4@T_m$ units were analyzed in an attempt to load the T_{10} cage with a greater number of hydrogen atoms. These computations yielded $OsH_4@T_{10}$ as the only exothermic system within this group of metal atoms. Within the cage, the Os—H bond length was found to be significantly reduced when compared with the free OsH_4 molecule. No exothermic solutions were identified for $MH_6@T_{10}$.

It will be interesting to continue this work by considering larger POSS cages than T_8 and T_{10} as enclosures for MH_{2n}, in particular T_{12} [30,40], and simultaneously assess their capabilities for hosting more complex metal polyhydrides than considered in the present work. Predictions based on such a modeling effort might create a strong incentive to explore routes for synthesis of $MH_{2n}@T_m$ composites with $n \geqslant 3$ and $m \geqslant 12$.

The results presented here make it appear plausible that POSS cages encapsulating metal hydrides may be stable and contain the hydrogen subsystem in a more compact form than the gas phase molecule.

Acknowledgment

We gratefully acknowledge support from the Tennessee NSF-EPSCoR Grant TN-SCORE (NSF EPS 1004083).

Appendix A. Supplementary data

Supplementary data associated with this article can be found, in the online version, at http://dx.doi.org/10.1016/j.chemphys.2013.09.003.

References

[1] S. Patchkovskii, J.S. Tse, S.N. Yurchenko, L. Zhechkov, T. Heine, G. Seifert, PNAS 102 (2005) 10439.
[2] L. Gagliardi, J. Chem. Theory Comput. 1 (2005) 1172.
[3] L. Gagliardi, P. Pyykkö, J. Am. Chem. Soc. 126 (2004) 15014.
[4] S. Erkoc, L. Turker, J. Mol. Struct. Theochem. 634 (2003) 195.
[5] H. Dodziuk, L. Dolgonos, O. Lukin, Carbon 39 (2001) 1907.
[6] O. Charkin, N. Klimenko, D. Charkin, A. Mebel, Zh. Neorg. Khim. 49 (2004) 792.
[7] O. Charkin, N. Klimenko, D. Charkin, A. Mebel, Zh. Neorg. Khim. 49 (2004) 953.
[8] A. Rehaman, L. Gagliardi, P. Pykko, Int. J. Quant. Chem. 107 (2007) 1162.
[9] X. Peng, X.J. Li, D.X. Zhang, Y. Zhang, Struct. Chem. 20 (2009) 789.
[10] G. Li, L. Wang, H. Ni, C.U. Pittman Jr., J. Inorg. Organomet. Polym. 11 (2002) 123.
[11] J.F. Brown Jr., J. Am. Chem. Soc. 87 (1965) 4313.
[12] B. Dance, Semicond. Int. 24 (2001) 46.
[13] F.J. Feher, K.D. Wyndham, Chem. Commun. (1998) 323.
[14] G.Z. Li, L. Wang, H. Toghiani, T.L. Daulton, K. Koyama, C.U. Pittman Jr., Macromolecules 34 (2001) 8686.
[15] G.Z. Li, L. Wang, H. Toghiani, T.L. Daulton, C.U. Pittman, Polymer 43 (2002) 4167.
[16] H. Li, M. Eddaouddi, D.A. Richardson, O.M. Yaghi, J. Am. Chem. Soc. 120 (1998) 8567.
[17] N. Maxim, H.C.L. Abbenhuis, P.J. Stobbelaar, B.L. Mojet, R.R. van Santen, Phys. Chem. Chem. Phys. 18 (1999) 4473.
[18] N. Maxim, P.C.M.M. Magusin, P.J. Kooyman, J.H.M.C. van Wolput, R.A. van Santen, H.C.L. Abbenhuis, Chem. Mater. 13 (2001) 2958.
[19] K. Wada, K. Yamada, T. Kondo, T.-A. Mitsudo, Chem. Lett. (2001) 12.
[20] M.H. Lamm, T. Chen, S.C. Glotzer, Nano Lett. 3 (2003) 989.
[21] A. Romo-Uribe, P.T. Mather, T.S. Haddad, J.D. Lichtenhan, J. Polym. Sci. B Polym. Phys. 36 (1998) 1857.
[22] B.X. Fu, B.S. Hsiao, H. White, M. Rafailovich, P.T. Mather, H.G. Jeon, S. Phillips, J. Lichtenhan, J. Schwab, Polym. Int. 49 (2000) 437.
[23] A. Lee, J.D. Lichtenhan, J. Appl. Polym. Sci. 73 (1999) 1993.
[24] T.S. Haddad, J.D. Lichtenhan, Macromolecules 29 (1996) 7302.
[25] J.J. Schwab, J.D. Lichtenhan, Appl. Organomet. Chem. 12 (1998) 707.
[26] A. Maiti, R.H. Gee, R. Maxwell, A.P. Saab, Chem. Phys. Lett. 440 (2007) 244.
[27] M. Mattori, K. Mogi, Y. Sakai, T. Isobe, J. Phys. Chem. A 104 (2000) 10868.
[28] D.M. Hossain, C.U. Pittman, S. Saebo, F. Hagelberg, J. Phys. Chem. C 111 (2007) 6199.
[29] D.M. Hossain, C.U. Pittman, F. Hagelberg, S. Saebo, J. Phys. Chem. C 112 (2008) 16070.
[30] D.M. Hossain, F. Hagelberg, S. Saebo, C.U. Pittman, J. Inorg. Organomet. Polym. 20 (2010) 1574.
[31] S.S. Park, C. Xiao, F. Hagelberg, D.M. Hossain, C.U. Pittman, S. Saebo, J. Phys. Chem. A 108 (2004) 11260.
[32] C. Lee, W. Yang, R.G. Parr, Phys. Rev. B 37 (1988) 785.
[33] A.D. Becke, J. Chem. Phys. 98 (1993) 5648.
[34] W.J. Stevens, H. Basch, M. Krauss, J. Chem. Phys. 81 (1984) 6026.
[35] J.R. Barron, A.R. Kelley, R. Liu, J. Chem. Phys. 108 (1998) 1.
[36] J.A. Platts, J. Molec, Struct. (Theochem) 545 (2001) 111.
[37] K.W. Toernroos, Acta Crystallogr. C50 (1994) 1646.
[38] P.A. Agaskar, W.G. Klemperer, Inorg. Chim. Acta 229 (1995) 255.
[39] The three geometric prototypes are shown in the supporting information (Figure S-2), which displays the optimization results obtained for OsH4..
[40] J.R. Cheeseman, G.W. Trucks, T. Keith, M.J. Frisch, J. Phys. Chem. 104 (1996) 5497.